A Numerical Investigation of Flow and Performance Characteristics of a Small Propeller Fan Using Viscous Flow Calculations

Keon-Je Oh*
Department of Mechanical Engineering, Kyungnam University, Wolyoung-Dong 449, Masan, Kyungnam 631-701, Korea
Shin-Hyoung Kang
Department of Mechanical Engineering, Seoul National University, Shinrim-Dong, Seoul 151-742, Korea

The present work is aimed at investigating an unusual variation in flow and performance characteristics of a small propeller fan at low flow rates. A performance test of the fan showed dual performance characteristics, i.e., radial type characteristics at low flow rates and axial type at high flow rates. Dual performance characteristics of the fan are numerically investigated using viscous flow calculations. The Finite Volume Method is used to solve the continuity and Navier-Stokes equations in the flow domain around a fan. The performance parameters and the circumferentially averaged velocity components obtained from the calculations are compared with the experimental results. Numerical values of the performance parameters show good agreement with the measured values. The calculation simulates the steep variations of performance parameters at low flow rates and shows the difference in the flow structure between high and low flow rates. At a low flow coefficient of $\Phi=0.2$, the flow enters the fan in an axial direction and is discharged radially outward at its tip, which is much like the flow characteristics of a centrifugal fan. The centrifugal effect at low flow rates makes a significant difference in performance characteristics of the fan. As the inlet flow rate increases, flow around the fan changes into the mixed type at $\Phi=0.24$ and the axial discharge at $\Phi=0.4$.

Key Words: Propeller Fan, Viscous Flow, Performance, Flow Field

Nomenclature

B_i^j	: Transformation matrix
D_P	: Fan diameter
G^i	: Contravariant velocity component
J	: Jacobian
k	: Turbulence kinetic energy
N	: Number of rotation per second (rev/s)
p	: Pressure
P_P	: Fan power
Q	: Volume flow rate
R_P	: Fan radius
Δp	: Static pressure rise
Re	: Reynolds number
S_ϕ	: Source term in the governing equations
(U, V, W)	: Velocity components in the rotating cylindrical coordinate
V_t	: Fan tip speed $(=\omega R_P)$
W_S	: Swirling velocity component in the fixed coordinate
(x, r, θ)	: Cylindrical coordinate
ε	: Dissipation rate of turbulence

* Corresponding Author,
E-mail: ohkj@kyungnam.ac.kr
TEL: +82-55-249-2616; **FAX**: +82-55-249-2617
Department of Mechanical Engineering, Kyungnam University, Wolyoung-Dong 449, Masan, Kyungnam 631-701, Korea. (Manuscript **Received** June 22, 2001; **Revised** December 19, 2001)

kinetic energy
Γ_ϕ : Diffusion coefficient
ϕ : Flow variable
Φ : Flow coefficient
Ψ : Head coefficient
Λ : Power coefficient
ω : Angular speed (rad/sec)
ρ : Density of the air
(ξ, η, ζ) : Body-fitted coordinate

1. Introduction

Propeller fans are commonly used for circulating room air or cooling electrical equipment. The flow around a fan is incompressible and shows complex aspects of turbulent viscous flow with re-circulation. Detailed study on these viscous flow characteristics is essential in order to predict fan performance and to improve fan efficiency. Flow computation methods for design purposes have mainly relied on the potential flow theory with empirical corrections for viscous effects. Inviscid flow calculations give reasonable results for pressure and velocity distributions in normal operation near the design condition, because the viscous effects are not dominant and confined in a small region near the wall surface. However, when the fan operates at off-design or abnormal conditions, flow field is strongly influenced by viscous effects and complicated by re-circulating flows. In such cases, viscous flow simulations are needed to predict the flow field.

Various viscous flow simulation methods were developed and validated for computation of flow and performance of turbomachines. Davis et al. (1988) predicted the performance of a two dimensional transonic compressor cascade over the entire range of incidence angle. Hobson and Lakshiminarayana (1991) used the incompressible Navier-Stokes techniques to predict the performance of two dimensional cascade for various incidence angles and numerical results were compared with the experimental data. Vu and Shyy (1994) investigated runner performance of two types of Fracis turbines using a viscous flow analysis and demonstrated that the viscous flow method is capable of yielding quite useful information about runner performance.

Recently, Kim (1998) reported an unusual variation of performance of a small propeller. The measurements indicated that there was a sudden rise in the head and the fan power at low flow rates, showing an S-shaped variation of the performance curve. He reported that a propeller fan, originally designed as an axial flow fan, actually operated like a radial flow fan at low flow rates. It is quite interesting to investigate the dual character of a small propeller fan at low and high flow rates.

The aim of the present work is to numerically investigate the dual character of a fan using viscous flow calculations. The computer code used here was developed by the authors and validated for propeller flow (Oh and Kang, 1995), which was quite similar to the flow around a fan. Performance parameters and the velocity components obtained from the viscous flow calculations are compared with the measured data to demonstrate the validity of this method. The flow field around the fan is examined to investigate a difference in regional flow characteristics between the low and high flow rates.

2. Governing Equations

Configuration of a flow model is shown in Fig. 1. A fan is operating at the inlet of circular chamber. The flow around the fan is an incompressible, viscous, and turbulent flow. The governing equations are the continuity and the Reynolds-averaged Navier-Stokes equations. The Reynolds stresses are modeled using the standard k-ε turbulence model. The governing equations in the rotating cylindrical coordinate can be written as

$$\frac{\partial}{\partial x}(U\phi)+\frac{1}{r}\frac{\partial}{\partial r}(rV\phi)+\frac{1}{r}\frac{\partial}{\partial\theta}(W\phi)= \frac{\partial}{\partial x}\left(\Gamma_\phi\frac{\partial\phi}{\partial x}\right)+\frac{1}{r}\frac{\partial}{\partial r}\left(r\Gamma_\phi\frac{\partial\phi}{\partial r}\right) +\frac{1}{r}\frac{\partial}{\partial\theta}\left(\frac{\Gamma_\phi}{r}\frac{\partial\phi}{\partial\theta}\right)+S_\phi \quad (1)$$

where ϕ, Γ_ϕ, and S_ϕ denote the flow variables, diffusion coefficients, and source terms, respec-

tively.

The flow domain is bounded by the blade passage, hub, inlet and outlet sections, and outer wall of the chamber. A non-orthogonal boundary-fitted coordinate system (ξ, η, ζ) is used to transform a physical domain into a rectangular computational domain. The transformation of the governing equations, leaving the flow variables in the original cylindrical coordinate, can be expressed as

$$\begin{aligned}&\frac{\partial}{\partial\xi}(G^1\phi)+\frac{\partial}{\partial\eta}(G^2\phi)+\frac{\partial}{\partial\zeta}(G^3\phi)\\&=\frac{\partial}{\partial\xi}\left(\frac{\Gamma_\phi}{J}B_1{}^1\frac{\partial\phi}{\partial\xi}\right)+\frac{\partial}{\partial\eta}\left(\frac{\Gamma_\phi}{J}B_2{}^2\frac{\partial\phi}{\partial\eta}\right)\\&+\frac{\partial}{\partial\zeta}\left(\frac{\Gamma_\phi}{J}B_3{}^3\frac{\partial\phi}{\partial\zeta}\right)+\frac{\partial}{\partial\xi}\left(\frac{\Gamma_\phi}{J}B_2{}^1\frac{\partial\phi}{\partial\eta}\right)\\&+\frac{\partial}{\partial\eta}\left(\frac{\Gamma_\phi}{J}B_3{}^2\frac{\partial\phi}{\partial\zeta}\right)+\frac{\partial}{\partial\zeta}\left(\frac{\Gamma_\phi}{J}B_1{}^3\frac{\partial\phi}{\partial\xi}\right)\\&+\frac{\partial}{\partial\xi}\left(\frac{\Gamma_\phi}{J}B_3{}^1\frac{\partial\phi}{\partial\zeta}\right)+\frac{\partial}{\partial\eta}\left(\frac{\Gamma_\phi}{J}B_1{}^2\frac{\partial\phi}{\partial\xi}\right)\\&+\frac{\partial}{\partial\zeta}\left(\frac{\Gamma_\phi}{J}B_2{}^3\frac{\partial\phi}{\partial\eta}\right)+JS_\phi\end{aligned}\tag{2}$$

where B_i^j is the transformation matrix represented by the partial derivatives of (x, r, θ) with respect to (ξ, η, ζ), J represents the Jacobian, G^i represents the contravariant velocity components, and S_ϕ represents the source terms in the governing equations.

3. Boundary Conditions

The boundary conditions are as follows.

(1) Inlet and outlet sections. The zero-gradient condition is specified for the flow variables, and the stream-wise velocity component is corrected in each iteration so that the flow rate is constant during the iterations.

(2) Blade, hub, and wall surface. The wall function method is employed. The first grid points next to the wall are placed in the logarithmic-law region, and correlations of the wall function (Gosmann and Ideriah, 1976) are imposed. A refined turbulence model using a sufficient number of grid points near the wall is needed to accurately simulate the boundary layer, including flow transition. In the present calculation, however, a rather simpler model is used because this study aims at investigating the overall flow field.

(3) Periodic surfaces. Periodic boundary conditions are given on the periodic surfaces.

(4) Wake centerline. Wake centerline conditions are given on the wake centerline.

4. Numerical Scheme

The governing equations are solved using the Finite Volume Method (Patankar, 1980). A set of discretization equations is obtained by integrating the governing equations over the individual control volume in a staggered grid system. Convection terms are calculated using a hybrid numerical scheme. Since the velocity field at each iteration does not satisfy the continuity equation, the velocity components are modified using the corrected pressure which has been determined in order to satisfy the continuity equation, i. e. , the SIMPLE algorithm (Patankar, 1980).

5. Calculation

5.1 Fan performance test

The fan model is 110mm in diameter, a four-bladed propeller fan commonly used for cooling an electrical equipment. The measurement for the present fan model was carried out by Kim (1998). In the test rig, a fan was placed at the inlet of a chamber, 3 m long and having a rectangular cross section of 900 mm x 900 mm. The outlet of the chamber was connected to a duct with a valve. The performance parameters of the fan and the velocity components at several radial and axial locations were measured with variation of rotational speeds.

The measured values at various rotational speeds show good agreement, and measurements at 2000 rpm are compared with the numerical results. The value of Reynolds number, based on the fan diameter and the blade tip speed at 2000 rpm, is $Re=1.2\times10^5$.

5.2 Computational model and grid system

The computational domain includes the fan and the front part of the chamber, as shown in

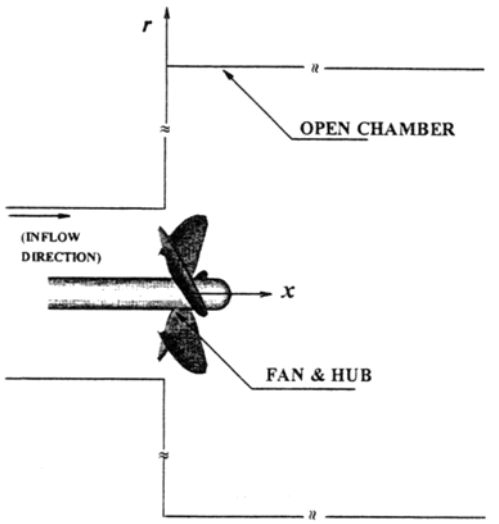

Fig. 1 Configuration of the flow model and coordinate system

Fig. 1. The outlet of the chamber is placed at eight fan diameters downstream of the fan. The outlet of the chamber in the calculation model is open and its size is about a quarter of that used in the test model. A circular chamber is assumed for rotational symmetry, while the chamber in the test rig has a square section. The inlet of the fan has a small entry duct for computational convenience.

The computational grid system has been generated for the calculation domain of the one blade passage using the algebraic generation method. The inlet boundary plane locates at $x/D_p=-0.5$, a half diameter upstream of the propeller, and the outlet boundary plane is at $x/D_p=8.0$, eight diameters downstream of the propeller. Two grid systems are tested to investigate the effect of grid refinement. The coarse and fine grids have (101, 44, 16) and (123, 57, 20) grid points, respectively. The fine grid spacing is used near the leading and trailing edges of the blade, the blade and hub wall surface, and the blade tip. Plane views of the computational grid for the coarse grid system are shown in Fig. 2. Test calculations are performed at $\Phi=0.24$, where the performance parameters show a sharp variation. Solutions are assumed to be converged when the residuals of the discretization equations are reduced to 1% of the reference value. The performance parameters and the circumferentially averaged velocity components at $x/D_p=0.185$ are chosen as reference variables to investigate grid

Table 1 Grid size effect on the calculated performane parameters for $\Phi=0.24$

Grid size	Flow coefficient	Head coefficient	Power coefficient
(101, 44, 16)	0.24	0.925	1.295
(123, 57, 20)	0.24	0.879	1.248

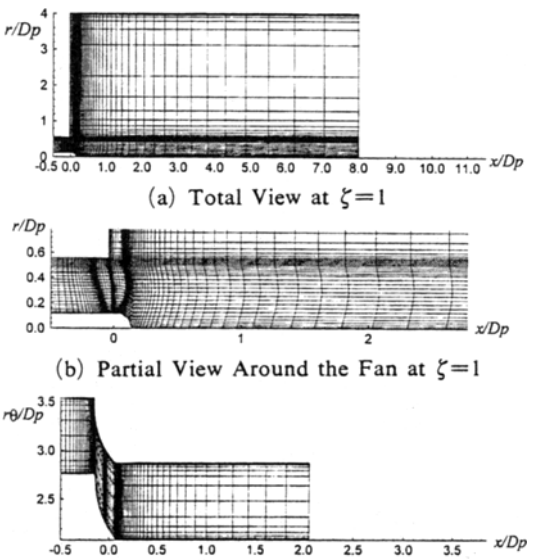

Fig. 2 Plane views of the grid construction

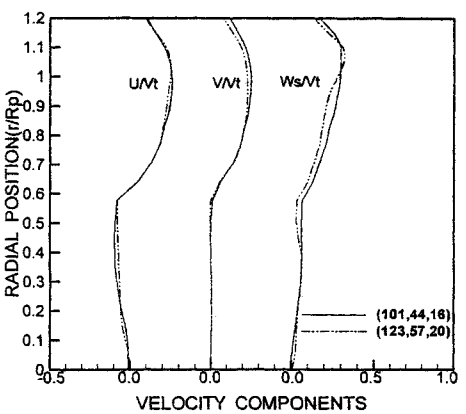

Fig. 3 Grid size effect on the calculated circumferentially averaged velocity components at $x/D_p=0.185$ for the flow coefficient of $\Phi=0.24$

independence. Table 1 shows the grid size effect on the calculated performance parameters for the flow coefficient of $\Phi=0.24$. Although the performance parameters sharply change at $\Phi=0.24$ in the performance curve, the grid refinement errors have been estimated within 5 %. Figure 3 also shows that the two grid systems yield nearly identical results for the velocity components, and no remarkable difference due to the grid refinement can be found. The following numerical results are calculated using a grid size of $(\xi, \eta, \zeta)=(101, 44, 16)$.

5.3 Results and discussion

Non-dimensional performance parameters, i.e., the flow coefficient Φ, the head coefficient Ψ, and the power coefficient Λ are defined as follows:

$$\Phi=\frac{Q}{ND_p^3},\ \Psi=\frac{\Delta p}{\rho N^2 D_p^5},\ \Lambda=\frac{P_p}{\rho N^3 D_p^5} \quad (3)$$

where Q is the volume flow rate, Δp the static pressure rise between the inlet and outlet boundary planes, P_p the fan power, N the number of rotations per second (rev/s), D_p the fan diameter, and ρ the density of the air.

Figures 4 and 5 show the performance characteristics with a variation of the head coefficients and the power coefficients, respectively, which represent the variations in static pressure rise and the fan power for different volume flow rates. It is observed from the measured data that the head coefficient and the power coefficient rapidly increase with a slight decrease in the flow coefficients around $\Phi=0.2$-0.3, showing an S-shaped characteristic curve. Also, the experimental data show an unusual trend in the characteristic curves and unstable bimodal operation at around $\Phi=0.2$-0.3. The head coefficient and the power coefficient increase with the flow coefficient, and there are two different values for the same flow rate. The rapid rise of the head coefficient and the power coefficient at a low flow rate near shut-off are uncommon features of the performance characteristics of the axial-type fan which arises from the centrifugal effect of the fluid; in other words, the flow at a low flow rate becomes much like that in a radial

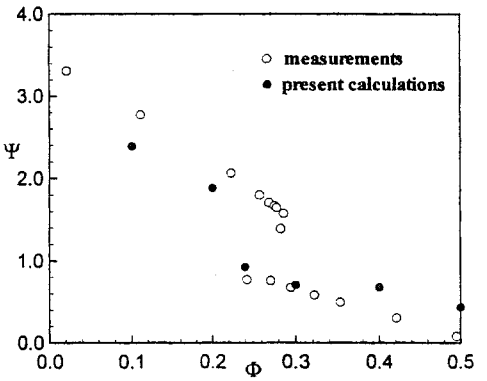

Fig. 4 Variations of the head coefficient for the different flow coefficients

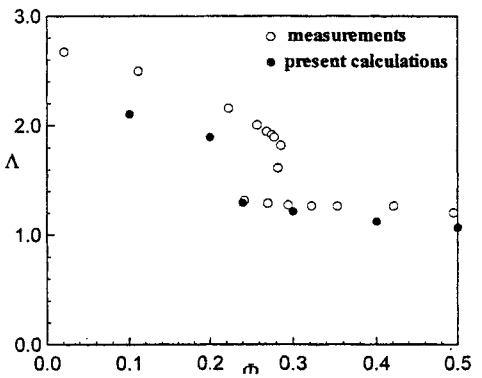

Fig. 5 Variations of the power coefficient for the different flow coefficients

fan. Comparisons between the predictions and the measurements show reasonable agreement. The predictions show sudden rise in the head and power coefficients when the flow coefficient decreases from 0.24 to 0.2. The calculated values show remarkable agreement with the measured characteristic curves. The differences between the predicted and experimental results are large at low flow rates because of complexity of the flow with re-circulating flows.

The flow field was investigated to find the characteristics of the flow at low and high flow rates. We used circumferentially-averaged velocities to find the flow structures in the axial and the radial flow directions. Figure 6 shows the vector plots and the stream-traces of the circumferentially averaged axial and radial velocity components around the fan region at a low

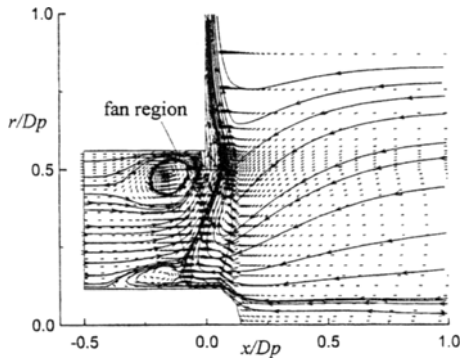

Fig. 6 Vector plots and streamtraces of the circumferentially averaged axial and radial velocities around the fan region for the flow coefficient of $\Phi=0.2$

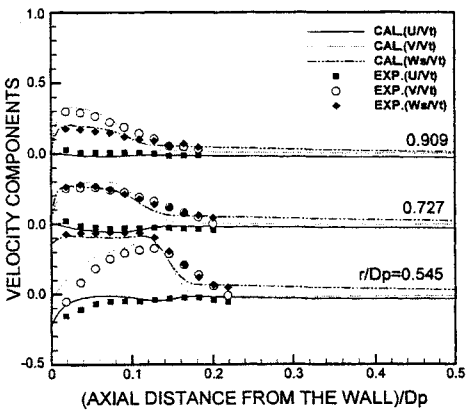

Fig. 7 Comparison of the measured and calculated circumferentially averaged velocity components at several radial positions for the flow coefficient of $\Phi=0.2$

flow coefficient of $\Phi=0.2$. The figure shows details of the flow at a low flow rate with the appearance of two re-circulating flow zones. The generation of a large central re-circulating zone behind the fan is due to swirling effect of the fan, which can be also observed in the swirling flow in a pipe expansion(Rhode et al., 1982). At a low flow rate of $\Phi=0.2$, the flow does not follow the axial streamlines in the fan region owing to the re-circulating flows. Instead, the radial velocity is much larger than the axial velocity, and the fluid moves along the radial streamlines. The streamlines show an inflow toward the hub, a radial outflow at the tip, and a change of the flow from an axial to a radial direction, which is much like that of a centrifugal fan. When the flow comes in axially toward the hub and goes out radially at the tip, there must be an angular momentum change by centrifugal effect between the inflow and the outflow. The centrifugal effect usually increases the static pressure rise at the same flow rate because the angular momentum change is larger than the axial momentum change. This indicates that the rapid rises of the power coefficient and the head coefficient, as shown in Figs. 4 and 5, are caused by the centrifugal effect.

Figure 7 shows the distribution of the velocity components at several radial positions for a low flow rate of $\Phi=0.2$. The velocity components are normalized by the fan tip speed V_t and plotted against the axial distance from the vertical wall of the chamber. The swirling velocity component W_s is defined in the fixed frame coordinate system. The radial position of $r/D_p=0.545$ is located in the tip gap. The measurements confirm that the flow is radially discharged. The radial velocity component is much larger than the axial velocity component. The discharged flow moves upward along the vertical wall of the chamber in the narrow flow region. The generation of the negative axial velocity component near the tip gap at $r/D_p=0.545$ shows the tip leakage flow in the tip clearance. The predictions agree very well with the measurements, thus indicating the validity of the numerical simulation.

Figure 8 shows the streamtraces of the circumferentially averaged velocity field for $\Phi=0.24$, where the performance parameters change sharply. The details of the flow structure become quite different from those at $\Phi=0.2$. The incoming flow toward the fan is uniform due to the removal of the re-circulating flow ahead of the fan. The extent of the central re-circulation zone is reduced owing to appearance of another re-circulating flow near the vertical wall of the chamber. The re-circulation zone penetrates into the tip, showing the turning of the tip leakage flow toward the exit of the fan. The flow at the exit of the fan is discharged with a flow angle, resulting in a mixed type between the axial and

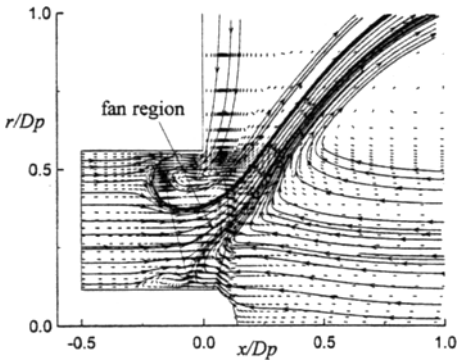

Fig. 8 Vector plots and streamtraces of the circumferentially averaged axial and radial velocities around the fan region for the flow coefficient of $\Phi=0.24$

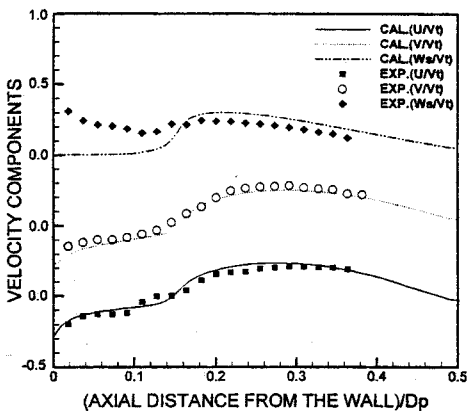

Fig. 9 Comparison of the measured and calculated circumferentially averaged velocity components at $r/D_p=0.545$ for the flow coefficient of $\Phi=0.24$

radial discharges.

Figures 9 and 10 show the distributions of the calculated and measured velocity components for $\Phi=0.24$ at $r/D_p=0.545$ and $x/D_p=0.185$, respectively. The radial position of $r/D_p=0.545$ locates in the tip gap. The axial position of $x/D_p=0.185$ is near the exit of the fan. The radial and axial velocity components at $r/D_p=0.545$ reverse in sign between the axial position of $x/D_p=0.1$ and 0.2. This indicates the flow turning near the tip, as captured in the calculated streamlines shown in Figure 8. The axial and radial velocity components at $x/D_p=0.185$ show similar distribution in both variation and magnitude, which illustrate the mixed type of flow discharge. The extent of the flow reversal zone is up to about one half of fan diameter at $x/D_p=0.185$. The calculated results are in reasonable agreement with the experimental results to validate the present computational results. The swirling velocity component at $r/D_p=0.545$ is under-predicted in the region where the radial velocity component is negative, i. e. , the flow moves downward. This difference mainly arises from the fact that the swirling effect of the fan in the downstream of the radial flow is not correctly taken into account because the present numerical method adopt the hybrid scheme with the upwind difference of convection terms.

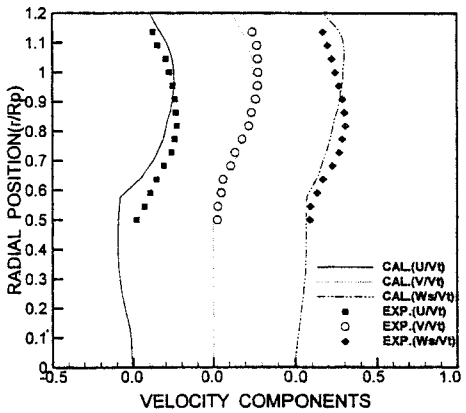

Fig. 10 Comparison of the measured and calculated circumferentially averaged velocity components at $x/D_p=0.185$ for the flow coefficient of $\Phi=0.24$

Figure 11 shows the streamtraces of the circumferentially averaged velocity field for a high flow rate of $\Phi=0.4$. As the inlet flow rate increases, the flow becomes nearly parallel to the axial direction. The re-circulating flow over the axis is much reduced and confined in a small region at the hub. On the other hand, the re-circulating zone on the vertical wall develops downstream of the flow. The flow follows the axial streamlines in the fan region with the axial momentum change between the inflow and the outflow, resulting in a decrease in static pressure rise and power. The tip flow feature with the flow turning is similar to that of $\Phi=0.24$.

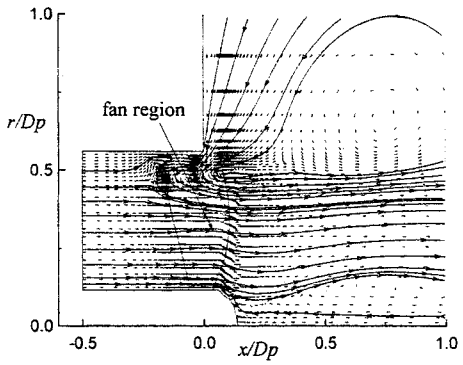

Fig. 11 Vector plots and streamtraces of the circumferentially averaged axial and radial velocities around the fan region for the flow coefficient of $\Phi=0.4$

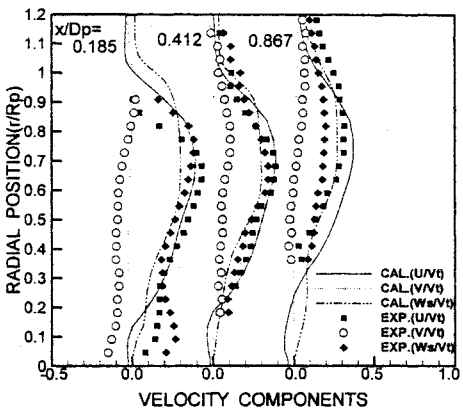

Fig. 12 Comparison of the measured and calculated circumferentially averaged velocity components at several axial positions for the flow coefficient of $\Phi=0.4$

Figure 12 shows the distributions of the calculated and measured velocity components for $\Phi=0.4$ at several axial positions. The magnitude of radial velocity component is nearly zero in the flow region and the flow is axially discharged, as observed in the streamline pattern. The flow stream is confined in the slipstream of the propeller wake with a size equal to about one diameter of the fan. The calculated results show reasonable agreement with the experimental results at $x/D_p=0.185$ and 0.412. However, the flow reversal near the hub at $x/D_p=0.185$ is not found in the measurements. The difference between the predictions and the measurements is large at the edge of the slipstream and the further downstream of $x/D_p=0.867$. These differences are associated with the numerical scheme, the limitation of the isotropic turbulence model, and insufficient grid resolution.

6. Conclusion

In the present study, the Navier-Stokes computation method is applied to calculate the viscous flow around a propeller fan operating at the inlet of an open chamber. The performance parameters and the flow structures are investigated with a variation of the flow rate. The predicted results are compared with the experimental results. From the forgoing discussions about the calculations and the measurements, the following conclusions can be drawn:

(1) The present calculations can handle the unusual variation of the performance at the low flow rates near shut-off, i. e., the sharp increase in the head coefficient and the power coefficient. The predictions show that the head and power coefficients sharply rise when the flow coefficient is decreased from 0.24 to 0.2, and the predicted values reproduce the characteristic curves obtained by the measurements.

(2) The rapid rise of the head and power coefficients at low flow rates is due to the centrifugal effect of the fluid. At a low flow coefficient of $\Phi=0.2$, the flow shows an inflow toward the hub and a radial outflow at the tip, which makes an angular momentum change in the flow between the inlet and the outlet of the fan. This is likely to cause a rapid increase in static pressure rise and fan power.

(3) The comparison of the measured and calculated velocity components give a good understanding of the flow structure at low and high flow rates. At $\Phi=0.2$, the flow is radially discharged at the tip and moves upward along the vertical wall of the chamber. As the flow coefficient increases, the flow changes to the axial discharge at $\Phi=0.4$ through a mixed type of the radial and axial discharge at $\Phi=0.24$. At $\Phi=$ 0.24 and 0.4, the re-circulating flow penetrates

into the tip region, showing a turning of the tip leakage flow toward the exit of the fan.

References

Davis R. L., Hobbs D. E., and Weingold H. D., 1988, "Prediction of Compressor Cascade Performance Using a Navier-Stokes Technique," *ASME J. of Turbomachinery*, Vol. 110, pp. 520 ~531.

Gosmann A. D., and Ideriah F. J. K., 1976, *TEACH-2E Computation Code Manual*, Dept. of Mechanical Engineering, Imperial College, England.

Hobson G. V., and Lakshiminarayana B., 1991, "Prediction of Cascade Performance Using an Incompressible Navier-Stokes Technique," *ASME J. of Turbomachinery*, Vol. 113, pp. 561 ~572.

Kim J., 1998, "Performance and Flow Characteristics of Forward Sweep Propeller Fan," Ph. D. Thesis, Dept. Mechanical Engineering, Seoul National University, Seoul, South-Korea.

Oh K., and Kang S., 1995, "Numerical Calculation of the Viscous Flow Around a Propeller -Shaft Configuration," *Int. J. for Numerical Methods in Fluids*, Vol. 21, No. 1, pp. 1~13.

Patankar S. V., 1980, *Numerical Heat Transfer and Fluid Flow*, McGraw-Hill Book Company, New York.

Rhode D. L., Lilley D. G., and McLaughlin D. K., 1982, "On the Prediction of Swirling Flow Fields Found in Axisymmetric Combustor Geometries," *ASME J. of Fluids Engineering*, Vol. 104, pp. 378~392.

Vu T. C., and Shyy W., 1994, "Performance Prediction by Viscous Flow Analysis for Francis Turbine Runner," *ASME J. of Fluids Engineering*. Vol. 116, pp. 116~120.